Graphene-based perfect optical absorbers harnessing guided mode resonances

M. Grande,[1,*] M. A. Vincenti,[2] T. Stomeo,[3] G. V. Bianco,[4] D. de Ceglia,[2] N. Aközbek,[5] V. Petruzzelli,[1] G. Bruno,[4] M. De Vittorio,[3,6] M. Scalora,[7] and A. D'Orazio[1]

[1] *Dipartimento di Ingegneria Elettrica e dell'Informazione, Politecnico di Bari, Via Re David 200, 70125 Bari, Italy*
[2] *National Research Council, Charles M. Bowden Research Center, RDECOM, Redstone Arsenal, Alabama 35898-5000 – USA*
[3] *Center for Bio-Molecular Nanotechnologies, Istituto Italiano di Tecnologia (IIT), Via Barsanti, 73010 Arnesano (Lecce), Italy*
[4] *Istituto di Nanotecnologia, Nanotec – CNR Via Orabona 4, 70126 Bari, Italy*
[5] *AEgis Technologies Inc, 410 Jan Davis Dr, Huntsville - AL, 35806, USA*
[6] *Dipartimento Ingegneria dell'Innovazione, Università Del Salento, Via Arnesano, 73100 Lecce, Italy*
[7] *Charles M. Bowden Research Center, RDECOM, Redstone Arsenal, Alabama 35898-5000 – USA*
[*] *marco.grande@poliba.it*

Abstract: We investigate graphene-based optical absorbers that exploit guided mode resonances (GMRs) attaining theoretically perfect absorption over a bandwidth of few nanometers (over the visible and near-infrared ranges) with a 40-fold increase of the monolayer graphene absorption. We analyze the influence of the geometrical parameters on the absorption rate and the angular response for oblique incidence. Finally, we experimentally verify the theoretical predictions in a one-dimensional, dielectric grating by placing it near either a metallic or a dielectric mirror, thus achieving very good agreement between numerical predictions and experimental results.

OCIS codes: (050.0050)_Diffraction and gratings; (130.3120) Integrated optics devices; (300.1030) Absorption.

References and links

1. S. Z. Butler, S. M. Hollen, L. Cao, Y. Cui, J. A. Gupta, H. R. Gutiérrez, T. F. Heinz, S. S. Hong, J. Huang, A. F. Ismach, E. Johnston-Halperin, M. Kuno, V. V. Plashnitsa, R. D. Robinson, R. S. Ruoff, S. Salahuddin, J. Shan, L. Shi, M. G. Spencer, M. Terrones, W. Windl, and J. E. Goldberger, "Progress, challenges, and opportunities in two-dimensional materials beyond graphene," ACS Nano **7**(4), 2898–2926 (2013).
2. R. R. Nair, P. Blake, A. N. Grigorenko, K. S. Novoselov, T. J. Booth, T. Stauber, N. M. R. Peres, and A. K. Geim, "Fine structure constant defines visual transparency of graphene," Science **320**(5881), 1308 (2008).
3. Y. D. Chong, L. Ge, H. Cao, and A. D. Stone, "Coherent perfect absorbers: time-reversed lasers," Phys. Rev. Lett. **105**(5), 053901 (2010).
4. W. Wan, Y. Chong, L. Ge, H. Noh, A. D. Stone, and H. Cao, "Time-reversed lasing and interferometric control of absorption," Science **331**(6019), 889–892 (2011).
5. M. Pu, Q. Feng, M. Wang, C. Hu, C. Huang, X. Ma, Z. Zhao, C. Wang, and X. Luo, "Ultrathin broadband nearly perfect absorber with symmetrical coherent illumination," Opt. Express **20**(3), 2246–2254 (2012).
6. M. Kang, Y. D. Chong, H.-T. Wang, W. Zhu, and M. Premaratne, "Critical route for coherent perfect absorption in a Fano resonance plasmonic system," Appl. Phys. Lett. **105**(13), 131103 (2014).
7. J. Zhang, C. Guo, K. Liu, Z. Zhu, W. Ye, X. Yuan, and S. Qin, "Coherent perfect absorption and transparency in a nanostructured graphene film," Opt. Express **22**(10), 12524–12532 (2014).
8. Y. Fan, Z. Liu, F. Zhang, Q. Zhao, Z. Wei, Q. Fu, J. Li, C. Gu, and H. Li, "Tunable mid-infrared coherent perfect absorption in a graphene meta-surface," http://arxiv.org/abs/1502.07435.
9. F. Liu, Y. D. Chong, S. Adam, and M. Polini, "Gate-tunable coherent perfect absorption of terahertz radiation in graphene," http://arxiv.org/abs/1402.2368.
10. W. W. Salisbury, US Patent No. 2599944 (1952).
11. J. Nath, E. Smith, D. Maukonen, and R. E. Peale, "Optical Salisbury screen with design-tunable resonant absorption bands," J. Appl. Phys. **115**(19), 193103 (2014).
12. V. Thareja, J. H. Kang, H. Yuan, K. M. Milaninia, H. Y. Hwang, Y. Cui, P. G. Kik, and M. L. Brongersma, "Electrically tunable coherent optical absorption in graphene with ion gel," Nano Lett. **15**(3), 1570–1576 (2015).
13. S. Thongrattanasiri, F. H. L. Koppens, and F. J. García de Abajo, "Complete optical absorption in periodically patterned graphene," Phys. Rev. Lett. **108**(4), 047401 (2012).

#238453 Received 22 Apr 2015; revised 10 Jun 2015; accepted 19 Jun 2015; published 4 Aug 2015

14. M. S. Jang, V. W. Brar, M. C. Sherrott, J. J. Lopez, L. K. Kim, S. Kim, M. Choi, and H. A. Atwater, "Tunable large resonant absorption in a midinfrared graphene Salisbury screen," Phys. Rev. B **90**(16), 165409 (2014).
15. R. Alaee, M. Farhat, C. Rockstuhl, and F. Lederer, "A perfect absorber made of a graphene micro-ribbon metamaterial," Opt. Express **20**(27), 28017–28024 (2012).
16. P. Y. Chen, M. Farhat, and H. Bağcı, "Graphene metascreen for designing compact infrared absorbers with enhanced bandwidth," Nanotechnology **26**(16), 164002 (2015).
17. H. A. Haus, *Waves and Fields in Optoelectronics* (Prentice Hall, 1984).
18. J. R. Piper and S. Fan, "Total Absorption in a Graphene Monolayer in the Optical Regime by Critical Coupling with a Photonic Crystal Guided Resonance," ACS Photonics **1**(4), 347–353 (2014).
19. J. R. Tischler, M. S. Bradley, and V. Bulović, "Critically coupled resonators in vertical geometry using a planar mirror and a 5 nm thick absorbing film," Opt. Lett. **31**(13), 2045–2047 (2006).
20. J.-T. Liu, N.-H. Liu, J. Li, X. Jing Li, and J.-H. Huang, "Enhanced absorption of graphene with one-dimensional photonic crystal," Appl. Phys. Lett. **101**(5), 052104 (2012).
21. M. A. Vincenti, D. de Ceglia, M. Grande, A. D'Orazio, and M. Scalora, "Nonlinear control of absorption in one-dimensional photonic crystal with graphene-based defect," Opt. Lett. **38**(18), 3550–3553 (2013).
22. R. Magnusson and S. S. Wang, "New principle for optical filters," Appl. Phys. Lett. **61**(9), 1022 (1992).
23. A. Hessel and A. A. Oliner, "A new theory of wood's anomalies on optical gratings," Appl. Opt. **4**(10), 1275 (1965).
24. U. Fano, "Effects of configuration interaction on intensities and phase shifts," Phys. Rev. **124**(6), 1866–1878 (1961).
25. S. Fan and J. D. Joannopoulos, "Analysis of guided resonances in photonic crystal slabs," Phys. Rev. B **65**(23), 235112 (2002).
26. M. Grande, M. A. Vincenti, T. Stomeo, G. V. Bianco, D. de Ceglia, N. Aközbek, V. Petruzzelli, G. Bruno, M. De Vittorio, M. Scalora, and A. D'Orazio, "Graphene-based absorber exploiting guided mode resonances in one-dimensional gratings," Opt. Express **22**(25), 31511–31519 (2014).
27. E. D. Palik and G. Ghosh, *Handbook of Optical Constants of Solids* (Academic, 1998), Vol. **3**.
28. M. Bruna and S. Borini, "Optical constants of graphene layers in the visible range," Appl. Phys. Lett. **94**(3), 031901 (2009).

1. Introduction

During the few last years, two-dimensional materials have attracted considerable interest due to their unprecedented properties [1]. The experimental isolation of the first two-dimensional material, graphene, has accelerated different research lines in this new field, paving the way for new photonic applications and functionalities [2].

In this framework, devices devoted to light absorption played an important role thanks to high monolayer graphene absorption that reaches a constant value of about 2.3% over the visible range [2], well above the absorption of metallic and dielectric materials having similar thickness. However, when perfect absorption (or total light absorption, TLA) is required, several approaches have been proposed to achieve 100% absorption. One solution relates to coherent perfect absorption (CPA) where a lossy slab, illuminated on both sides, can absorb all the incoming light since it acts as an "anti-laser" [3–5]. In this case, the amplitudes and the phases of both beams must be controlled in order to achieve coherent absorption (or an absorptive interferometer). Furthermore, material absorption does not need to be necessarily high, therefore it may show a low single-pass absorption rate (e.g. wavelength range close to the transparent range). For example, in [3], Y. D. Chong et al detail how a 100 μm-thick silicon slab, working at ~945 nm (where the silicon extinction coefficient k is extremely low, i.e., $8 \cdot 10^{-4}$) is able to totally absorb the incoming light at a specific wavelength (making the device narrow-band).

This system is equivalent to a two-port optical system and the CPA phenomenon is related to the poles and zeros (i.e. singularities) of its (*non hermitian*) scattering matrix S with respect to the input and the output fields. When CPA constrains are satisfied, the combination of interference and dissipation (lossy slab) leads to perfect absorption. This approach overcomes the maximum achievable absorption, equal to 50%, when only a single input beam is considered in symmetric configurations. Finally, we note that this phenomenon does not require resonant structures with high Q factor (Q factor is about 840 in [4]) or surface nano-structuring. Instead, it requires slabs that are much thicker than the incident wavelength (for example, 100μm and 900nm, respectively) and necessitates complete control of intensity and

#238453 Received 22 Apr 2015; revised 10 Jun 2015; accepted 19 Jun 2015; published 4 Aug 2015

phase of the incoming beams in the two-port system. A similar approach has been recently proposed in [6] for thin meta-materials but, in this case, a plasmonic thin film was patterned in order to satisfy the CPA conditions.

To date, CPA in graphene has been efficiently achieved only in the THz regime [7–9], since its optical parameters and its thickness do not satisfy CPA conditions in the visible range. However, it is possible to reduce the complexity of the CPA systems to one-port systems by adding a perfect mirror to the two-port system: intuitively, in this case, the perfect mirror reflects the transmitted light, which in turn, generates the incoming beam at the second port. In this one-port system, the absorption A is equal to $A = 1\text{-}R$, where R is the reflectance and the transmission channel T is suppressed ($T = 0$). Therefore, also in this one-port system, interference and absorption can again be "mixed" and designed to achieve a null reflectance that leads to perfect absorption or total light absorption.

One example corresponds to the "Salisbury screen" (SS) in the microwave regime [10] that is essentially constituted by a mirror, a lossless spacer and a thin absorbing layer. In particular, a fraction of the input beam that is transmitted into the spacer undergoes multiple partial reflections by resonating between the absorbing layer/spacer interface and the mirror. The total reflected beam can be designed to destructively interfere attaining total absorption of the incoming light. Recently, different schemes, based on the SS configuration, have been proposed in the optical regime [11–16]: in particular, in configurations based on graphene, the bi-dimensional layer plays only the role of the thin absorbing material (non-patterned graphene) [12] or adds a resonant structure due to its plasmonic nature (patterned graphene) [13, 14].

Since all these (CPA and SS) configurations define a cavity (e.g. an asymmetric Fabry-Pérot cavity with two mirrors having different reflectivities), they can also be analyzed in the domain of critical coupling [17, 18] as reported in [19] where a very thin absorbing film is placed on a dielectric Bragg reflector. However, the main drawback of the configurations reported in [12, 19] is that the optical Salisbury screen operates efficiently only at one wavelength value (at which destructive interference occurs) and, consequently, it cannot be tuned unless the refractive index, or alternatively the spacer thickness, is changed. In contrast, periodic structures allow phase matching and hence tuning of the operating wavelength.

Finally, when the graphene is employed as an absorbing film in the visible range, the lossless spacer and the dielectric mirror do not suffice to achieve perfect absorption as demonstrated in [20]. A solution may be found by adding a second mirror, as demonstrated in [21], where the graphene is sandwiched between two dielectric mirrors: the first one is a partially reflecting mirror, while the second mirror acts as a perfect mirror with high, near-100% reflectivity. The cavity enhances the electric field which in turn strongly interacts with the absorbing layer leading to resonant, cavity-enhanced absorption. Therefore, one may say that these results clearly show that is possible to employ graphene to achieve perfect absorption even if it displays low, single-pass absorption in different spectral ranges.

In this scenario, we propose to study optical absorbers that exploit guided mode resonances (GMRs) [22, 23], also known as Fano resonances [24, 25], in order to attain perfect absorption in the near-infrared (NIR) range. In particular, we combine a resonant, one-dimensional (1D) dielectric grating, with a reflection mirror separated by a lossless spacer. We point out that the 1D dielectric grating absorber without the mirror achieves a theoretical maximum absorption of about 60%, as recently demonstrated [26]. Furthermore, we consider the influence of the geometrical parameters of the 1D dielectric grating on the behavior of absorption and its angular response when the impinging source is tilted. Finally, we experimentally verify the theoretical assumption by realizing the 1D dielectric grating and placing it both on separate metallic and dielectric mirrors.

#238453 Received 22 Apr 2015; revised 10 Jun 2015; accepted 19 Jun 2015; published 4 Aug 2015

2. Numerical results

Figure 1(a) shows the sketch of the proposed configuration that is equivalent to a one-port system as described in the introduction. The mirror reflects the transmitted light, suppressing the transmission channel and generating a reflected beam towards the resonant structure.

Figure 1(b) details the geometrical parameters of the 1D dielectric grating-based absorber made of polymethyl-methacrylate (PMMA) stripes deposited on a tantalum pentaoxide (Ta_2O_5) slab that is supported by a silicon dioxide (SiO_2) substrate. The monolayer graphene is sandwiched between the polymeric layer and the Ta_2O_5 slab, forcing it to interact with the guided mode resonances. The Ta_2O_5 slab thickness t_{Ta2O5}, the periodicity p, the PMMA width w_{PMMA} and the PMMA thickness t_{PMMA} are initially set equal to 100 nm, 470 nm, 305 nm ($w_{PMMA} = 0.65p$) and 650 nm, respectively.

Finally, a semi-infinite flat mirror (either an ideal mirror or gold), that reflects the transmitted light, supports the 1D dielectric grating.

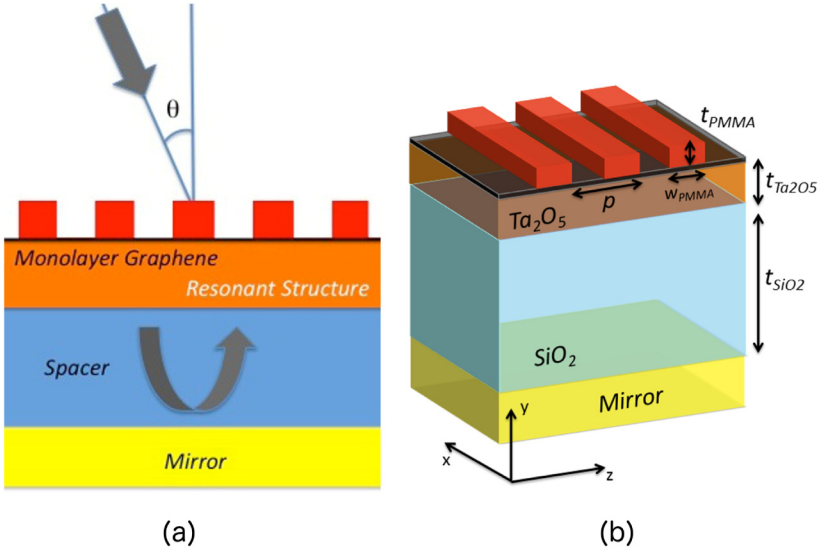

Fig. 1. (a) One-port system with a resonant structure, a spacer and a reflecting mirror. (b) Sketch of the 1D grating: PMMA stripes (red) on Ta_2O_5 slab (orange) grown on silicon dioxide substrate (cyan). The black thin layer indicates the monolayer graphene.

The simulations are performed using the Rigorous Coupled-Wave Analysis (RCWA) method. The refractive index of the dispersive materials (*PMMA*, Ta_2O_5, SiO_2 and *Au*) was retrieved by means of ellipsometric measurements. We found that the permittivity values do not differ from the data reported in [27] and the extinction coefficients for all the dielectric media (except for gold and the monolayer graphene) are almost zero, allowing us to deal with a lossless system. The monolayer graphene was described with a complex refractive index $\tilde{n} = 3 + jC_1\lambda/3$ (where C_1 is equal to 5.446 μm^{-1}) following the model reported in [28]. Hereinafter, we will only consider TE polarization (plane of incidence *yz* and electric field along *x*), although similar results and considerations are obtained for TM-polarized light.

We being our analysis by considering the 1D grating sketched in Fig. 1 supported by a perfect (ideal) electric mirror, or PEM (or perfect conductor). Fig. 2(a) and (b) show the absorption map and absorption maxima, in the presence of monolayer graphene, in the wavelength range of interest (0.6 μm – 0.8 μm) for the SiO_2 thickness t_{SiO2} varied in the range 0 – 0.4 μm at normal incidence. It is evident that the absorption wavelength shifts towards higher wavelengths as the SiO_2 layer thickness is increased. Furthermore, the absorption Full-Width at Half-Maximum (FWHM), equal to about 4.4 nm, can be derived by inspecting Fig.

#238453 Received 22 Apr 2015; revised 10 Jun 2015; accepted 19 Jun 2015; published 4 Aug 2015

2(c) that shows the optical response, in terms of transmittance, reflectance and absorption, of the absorber at the second maximum (t_{SiO2} = 0.315 μm). Figure 2(c) also demonstrates that the absorption reaches 100% (43-fold increase with respect to bare graphene) at about 0.741 μm while transmittance and reflectance are null.

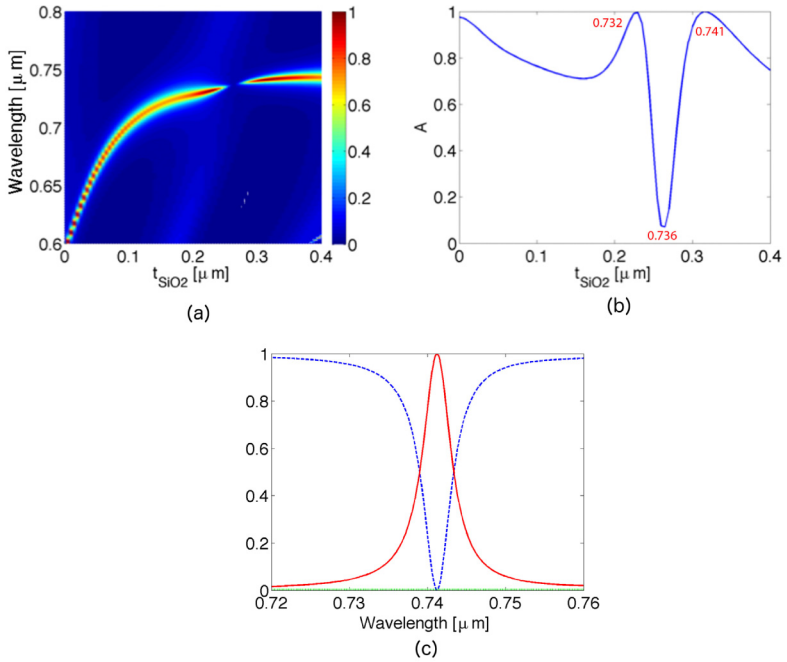

Fig. 2. (a) Absorption map versus the t_{SiO2} thickness for the PEM configuration, in presence of the monolayer graphene, at normal incidence, when the Ta_2O_5 slab thickness t_{Ta2O5}, the periodicity p, the PMMA width w_{PMMA} and the PMMA thickness t_{PMMA} are equal to 100 nm, 470 nm, 305 nm (w_{PMMA} = 0.65p) and 650 nm, respectively. (b) Maximum achievable absorption when the t_{SiO2} thickness is varied. The maxima and minima wavelengths (in micron) are indicated in red. (c) Reflectance (blue dashed curve), transmittance (green dotted curve) and absorption (red solid curve) spectra when the SiO_2 thickness t_{SiO2} = 0.315 μm.

At the same time, absorption varies between about 10% and perfect absorption: in particular, this configuration (Fig. 2(b)) shows two maxima (located at t_{SiO2} = 0.230 μm, and 0.315 μm) and one minimum (located at t_{SiO2} = 0.265 μm).

All the maxima correspond to a 43-fold increase compared to the isolated monolayer graphene absorption (2.3%) since the monolayer graphene is the only absorbing material in this configuration.

It is possible to verify that the distance between maxima (minima) (e.g. in Fig. 2(b)) corresponds to $\lambda/(2n_{SiO2})$ due to constructive (destructive) interference of the Fabry-Pérot cavity mode in the SiO_2 layer.

Figures 3(a) and (b) show the absorption map and absorption maxima, respectively, in the wavelength range of interest (0.6 μm – 0.8 μm), in presence of the monolayer graphene for each SiO_2 thickness t_{SiO2} in the range 0 – 0.3 μm, at normal incidence, when a gold mirror is considered. Also in this case, Figs. 3(a) and (b) show a similar behavior as in Figs. 2(a)-(b) with a shift of about 30 nm that is related to the complex reflection coefficient (due to the complex gold refractive index) that introduces a phase shift.

#238453 Received 22 Apr 2015; revised 10 Jun 2015; accepted 19 Jun 2015; published 4 Aug 2015

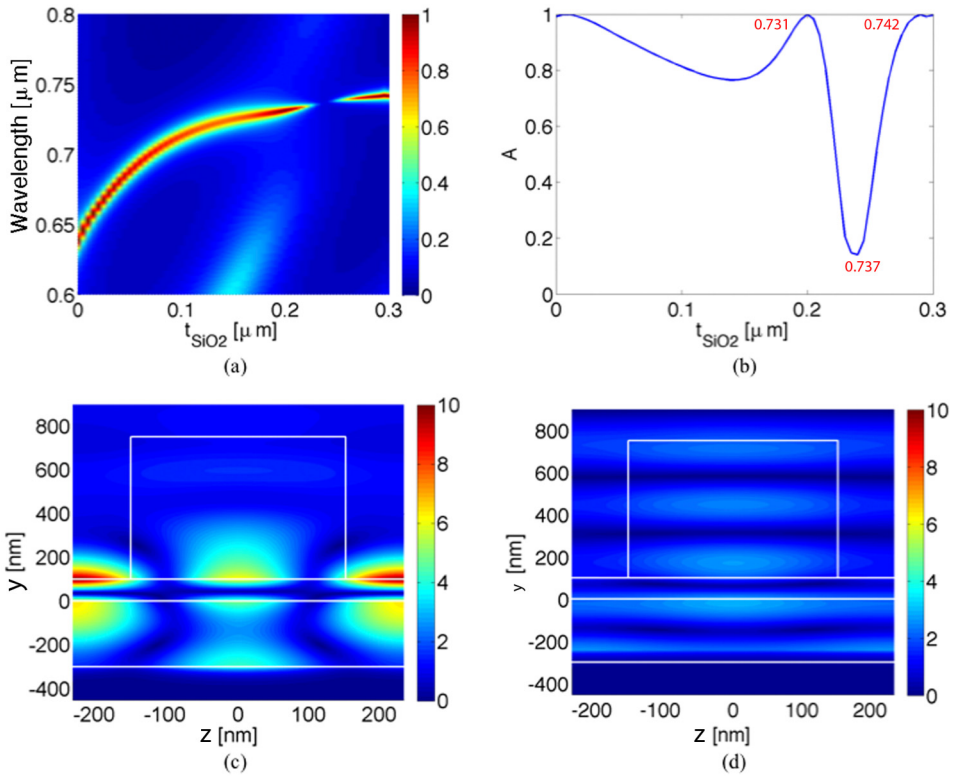

Fig. 3. (a) Absorption map versus the t_{SiO2} thickness and (b) its maximum at normal incidence, when the Ta_2O_5 slab thickness t_{Ta2O5}, the periodicity p, the PMMA width w_{PMMA} and the PMMA thickness t_{PMMA} are equal to 100 nm, 470 nm, 305 nm (w_{PMMA} = 0.65p) and 650 nm, respectively. is set equal to 0.65p. The maxima and minima wavelengths (in micron) are indicated in red. Magnetic field profile (amplitude of the H_z component) when t_{SiO2} is equal to (c) 0.3 μm at λ = 0.7418 μm and (d) 0.24 μm at λ = 0.7368 μm, respectively. The monolayer graphene is positioned at y = 0.1 μm (white horizontal line) while the gold layer is placed at y < –0.3 μm.

Moreover, this configuration allows one to achieve perfect absorption; this behavior can be easily explained by inspecting the magnetic field profile (H_z field component) at maximum absorption (t_{SiO2} = 0.3 μm) that reveals the localization of the field at the monolayer graphene position (y = 0.1 μm) as illustrated in Fig. 3(c). We note that the magnetic field penetrates into the metal layer (y < –0.3 μm) due to its finite conductivity. In contrast, the magnetic field profile of the configuration corresponding to the minimum of Fig. 3(b) shows that the field is localized in the SiO_2 spacer, scarcely interacting with the monolayer graphene (Fig. 3(d)). Lastly, if we fix the wavelength, i.e. λ = 0.7416 μm, absorption varies between 8.5% and 100% (Fig. 3(a)).

The performance of the 1D dielectric grating-based absorber, at normal incidence, when the PMMA width w_{PMMA} is varied is reported in Fig. 4. The spacer thickness is fixed equal to t_{SiO2} = 0.3 μm (Fig. 3(b)) so that the perfect absorption condition is fulfilled. In particular, Fig. 4(a) shows that absorption wavelength (0.737 μm at w_{PMMA} = *0.5p*, spanning in the range 0.735 μm - 0. 740 μm) and its FWHM (4.9 nm at w_{PMMA} = *0.5p)* are almost constant in the w_{PMMA} range 0.3p – 0.7p. This is also valid for the absorption that shows a maximum equal to 100% when w_{PMMA} = *0.65p* while it reaches 97.6% in the center (i.e. w_{PMMA} = *0.5p*) as evidenced in Fig. 4(b). This behavior confirms the stability of the proposed device against fabrication tolerances and proves a stable critical coupling over a wide range of the

#238453 Received 22 Apr 2015; revised 10 Jun 2015; accepted 19 Jun 2015; published 4 Aug 2015

geometrical parameters. It is worth noting that the leakage is proportional to the fill factor that in this case varies linearly with the PMMA width w_{PMMA}.

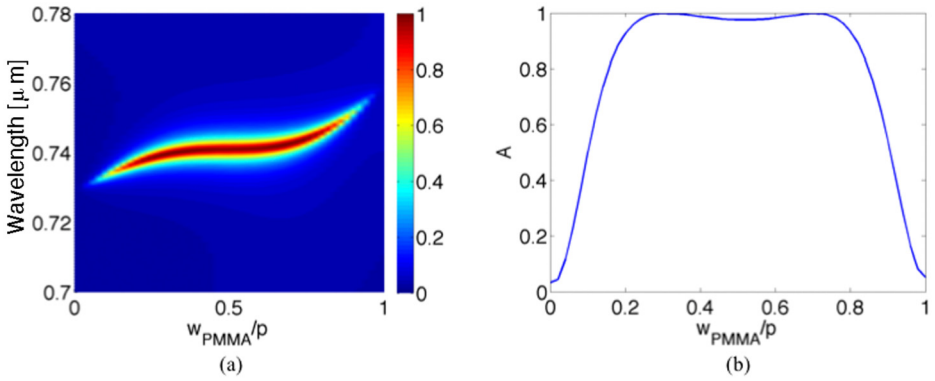

Fig. 4. (a) Absorption map and (b) maximum achievable absorption versus the PMMA width w_{PMMA} normalized to the periodicity p when t_{SiO2} = 0.3 μm and the monolayer graphene is taken into account. The Ta_2O_5 slab thickness t_{Ta2O5}, the PMMA width w_{PMMA} and the PMMA thickness t_{PMMA} are equal to 100 nm, 305 nm (w_{PMMA} = 0.65p) and 650 nm, respectively.

Up to now we have considered only the response of the optical absorbers at normal incidence. Since the proposed device is based on a grating configuration, we are also interested in its angular behavior. Figure 5(a) shows the absorption map when the incident angle θ (Fig. 1(a)) is varied in the range 0° - 20°. From an inspection of the plot, it is evident that the resonance at normal incidence splits in two arms when the source is tilted. Furthermore, the position of the two absorption peaks follows the dispersion of the guided mode resonance that introduces the rapid variation of the intensity in the spectrum. In particular, since we are in the zero-order diffraction regime (at the input interface) due to the sub-wavelength periodicity, the two arms follow the coupling, into the Ta_2O_5 slab, with the evanescent mode orders having m equal to +/−1. Figure 5(b) shows the dispersion relation for the GMR analytically calculated by considering the diffraction behavior of the four-layer structure.

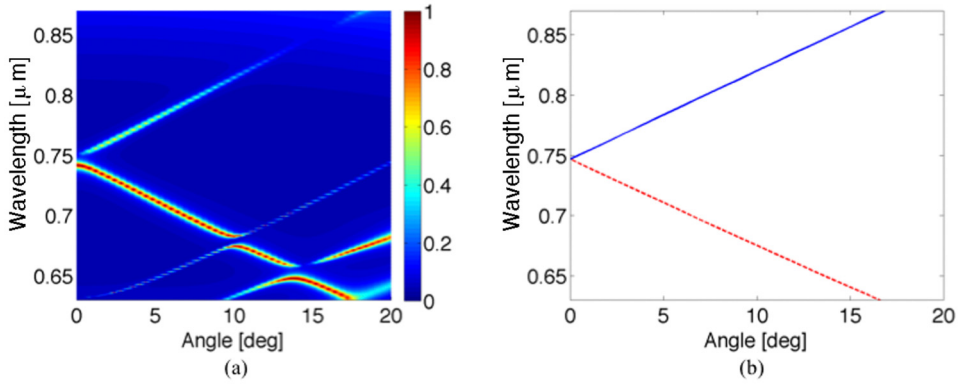

Fig. 5. (a) Angular dependence of the absorption when the incident angle θ is varied in the range 0° - 20° (the Ta_2O_5 slab thickness t_{Ta2O5}, the periodicity p, the PMMA width w_{PMMA} and the PMMA thickness t_{PMMA} are equal to 100 nm, 470 nm, 305 nm (w_{PMMA} = 0.65p) and 650 nm, respectively). (b) Guided resonance mode wavelength dispersion curve versus the angle of incidence for m = 1 (blue solid curve) and m = −1 (red dashed curve), respectively.

Finally, we note that: (i) the main feature of Fig. 5(a) is related to the asymmetric spectrum of the two arms that show different diffraction efficiencies; and (ii) even if the

#238453 Received 22 Apr 2015; revised 10 Jun 2015; accepted 19 Jun 2015; published 4 Aug 2015

proposed device is sensitive to incident source angle, one can reduce the angular dependence by working in a wavelength region where multiple anti-crossing points occur. For example, in the range 5°-20° absorption is limited between the narrow wavelength range 0.65 μm and 0.675 μm.

3. Fabrication and experimental results

In order to validate the theoretical results shown in the previous section, we initially fabricated the dielectric 1D grating on a 500 μm thick SiO_2 substrate. In particular, a 100 nm-thick Ta_2O_5 slab was grown on this substrate by means of a sputtering system while a Chemical Vapor Deposition (CVD) monolayer graphene was manually transferred onto the Ta_2O_5 slab. Then, the PMMA stripes, with a width w_{PMMA} and a periodicity p equal to $0.65p$ and 470 nm, were realized by means of an electron beam lithography system (Raith150) operating at 20 kV with an area dose equal to 300 μC/cm^2.

Figure 6 shows the Raman spectrum of the transferred monolayer graphene, after the fabrication process, proving the near-absence of defects (i.e. D peak at about 1350 cm^{-1}) and, hence, the preservation of the graphene quality during the fabrication process. The inset in Fig. 6 portrays the Scanning Electron Microscope (SEM) image of the 1D grating composed by the periodic PMMA stripes.

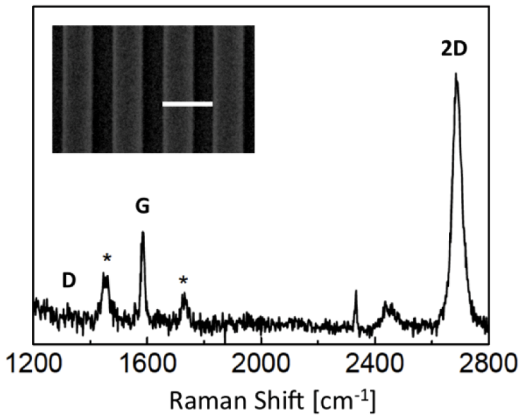

Fig. 6. Raman spectrum of the monolayer graphene after the fabrication process; the asterisks refer to the PMMA stripe spectral features; (inset) Scanning Electron Microscope (SEM) micrograph of the fabricated device where the white scalebar refers to 470 nm.

The configuration sketched in Fig. 1(a) may be realized by covering the SiO_2 substrate back-side with a metal layer. However, we decided to separate the mirror from the grating in order to use the same sample with different mirrors. In particular, we first placed the grating supported by the SiO_2 substrate on a 0.1μm-thick gold layer deposited on a silicon wafer.

We experimentally characterized the complete structure by means of an ad hoc optical setup. We shined white light on the sample by means of a 5x microscope objective, with a numerical aperture NA equal to 0.1. An optical iris spatially filtered the impinging light to select only the patterned area. Then, the reflected light was sent to an optical spectrometer (HR4000 from Ocean Optics) through collecting system composed by a multimode optical fiber and an aspherical lens.

For a full comparison of numerical and experimental results, we numerically analyzed the overall response of the measurement setup. Firstly, we defined the numerical reflectance spectrum of the device, with a periodicity p shifted by few nanometers, at normal incidence as shown in Fig. 7(a) (blue curve) with a spectral resolution of 0.2 nm; on the same plot, we superimposed a red curve that refers to a numerical average over N = 15 points (i.e. 3 nm).

#238453 Received 22 Apr 2015; revised 10 Jun 2015; accepted 19 Jun 2015; published 4 Aug 2015

Then, we considered the spectral response of the composed device when the incidence angle was varied in the range of the numerical aperture (Fig. 7(b)).

We considered also a modulation of the light in the numerical aperture cone with a Gaussian shape having a standard deviation σ equal to 3.4° (Fig. 7(c)). Multiplying the map shown in Fig. 7(b) by the amplitude modulation described in Fig. 7(c), we obtained the angular map depicted in Fig. 7(d).

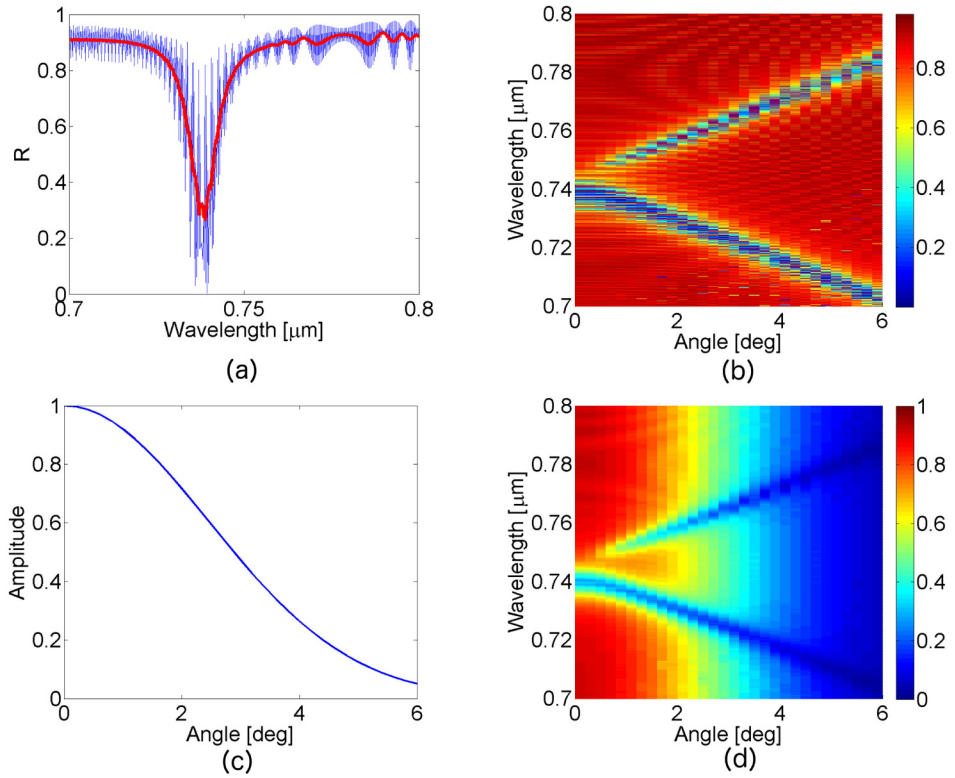

Fig. 7. (a) Normal incidence (blue curve) non-averaged reflectance and (thick red solid curve) averaged spectra of the composed device. (b) Angular response in the numerical aperture range with no averaging. (c) Modulation of the light in the numerical aperture cone (Gaussian with sigma = 3.4°). (d) Averaged and modulated angular response in the numerical aperture range.

Integrating over the angle range (i.e. x-axis of Fig. 7(d)), it is possible to retrieve the overall averaged response. In Fig. 8 the red dashed curve and the blue solid curve refer to numerical and experimental reflectance (Fig. 8(a)) and absorption (Fig. 8(b)) spectra, respectively. The comparison between experimental measurements and theoretical prediction shows very good agreement. These spectra also reveal an asymmetric dip and an asymmetric peak, respectively. This behavior is consistent with the asymmetry depicted in Fig. 5(a).

We note that Fig. 8 does not show perfect absorption since the grating is interrogated simultaneously at different angles, within the numerical aperture (Fig. 7(b)), leading to averaged spectra. Nevertheless, this indirectly demonstrates the absorption capability and behavior of the grating, as well as the reliability of the numerical approach. In order to overcome this limit and, hence, directly verify the perfect absorption behavior, one may employ a collimated beam (that illuminates the grating only at $\theta = 0$) for each wavelength (even if this is not straightforward in the visible-NIR range).

#238453 Received 22 Apr 2015; revised 10 Jun 2015; accepted 19 Jun 2015; published 4 Aug 2015

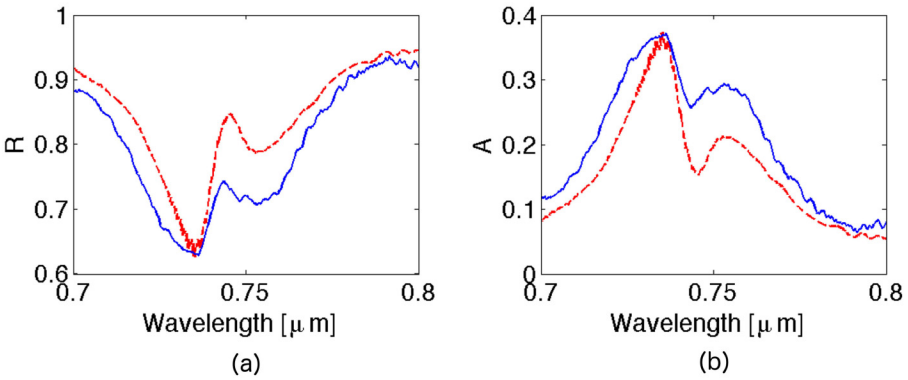

Fig. 8. Experimental (a) reflectance and (b) absorption spectra of the fabricated device (blue solid curves). For comparison, the red dashed curves refer to the numerical response.

Finally, as mentioned above, the fabrication of the 1D dielectric grating on a 500 μm thick SiO_2 substrate allowed us to change easily the reflecting mirror. In this regard, we also placed the grating on a commercial broadband dielectric mirror (BB05-E02 supplied by Thorlabs).

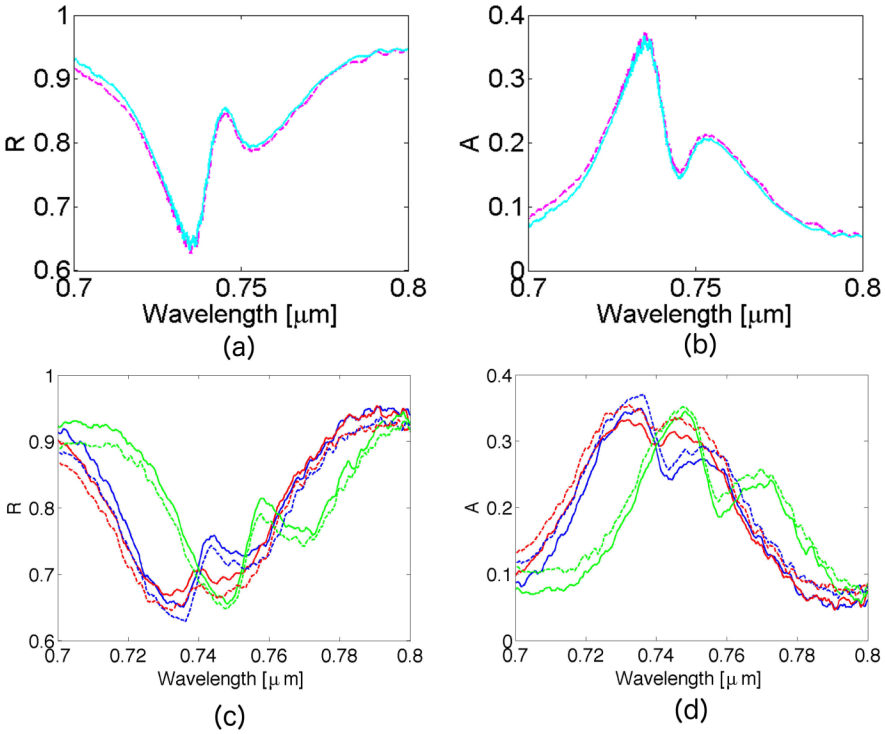

Fig. 9. Simulated (a) reflectance and (b) absorption spectra for the dielectric mirror (solid lines) and for the gold mirror (dashed lines), respectively. Measured (c) reflectance and (d) absorption spectra when the dose is equal to 250 μC/cm^2 (red curve), 300 μC/cm^2 (blue curve) and 350 μC/cm^2 (green curve) for the dielectric mirror (solid lines) and for the gold mirror (dashed lines), respectively.

Figures 9(a) and (b) show the numerical reflectance and the absorption spectra of the composed device for both the broadband dielectric mirror (solid lines) and gold layer (dashed lines). The comparison reveals that the two mirrors show almost identical response and, hence, validates the possibility to interchange different dielectric or metallic reflecting

#238453 Received 22 Apr 2015; revised 10 Jun 2015; accepted 19 Jun 2015; published 4 Aug 2015

mirrors. This behavior may be explained by first considering that the thick substrate prevents the change of the effective refractive index of the grating by the presence of the mirror; furthermore, the mirrors only introduce a phase shift that is averaged.

Finally, Figs. 9(c) and (d) show the experimental reflectance and absorption spectra of the same device for both the broadband dielectric mirror (solid lines) and gold layer (dashed lines). In the same plots we also considered two different structures, one with lower dose (250 $\mu C/cm^2$, red curves) and one with higher dose factor (350 $\mu C/cm^2$, green curves) revealing a slight shift with respect to the case we simulated (300 $\mu C/cm^2$, blue curves). The comparisons between Figs. 9(a) and (b) and the blue curves in Figs. 9(c) and (d) show very good agreement.

4. Conclusion

In conclusion, we have detailed the numerical analysis and the experimental verification of an optical absorber that exploits GMRs in order to attain perfect absorption. Our numerical findings reveal that the use of a lossless spacer and an ideal mirror is sufficient to achieve perfect absorption with a 40-fold increase of the monolayer graphene absorption over a bandwidth of ~5 nm. Similar behavior is found when a gold mirror replaces the ideal mirror. In this case, the minimum whole thickness of the optical absorber is equal to only about 1 μm.

Then, the angular dependence analysis reveals an asymmetric absorption response that follows the guided mode resonance due to the presence of the PMMA grating. Furthermore, even if this is beyond the scope of this work, the angular dependence may be "reduced" by exploiting the multiple anti-crossing regions in the diffraction curves, leading to almost angular insensitive optical absorbers.

From an experimental point of view, we fabricated the 1D dielectric grating and placed it on top of two different mirrors, a gold and a dielectric mirror, achieving very good agreement between experimental results and numerical simulations. We have also shown that this approach allows the interchange of mirrors, a fact that may be used to tune and switch between two different absorbing regimes with and without mirror.

The enormous advantage of the proposed geometry resides also in the possibility to directly deposit or transfer the monolayer graphene on a flat surface and not on a nanostructured surface, significantly reducing the number of issues relating to the fabrication process.

All these features clearly demonstrate that the proposed approach may be exploited to efficiently design and optimize graphene-based optical absorbers.

Acknowledgments

M. Grande thanks the U.S. Army International Technology Center Atlantic for financial support (W911NF-13-1-0434). This research was performed while the authors M. A. Vincenti and D. de Ceglia held National Research Council Research Associateship awards at the U. S. Army Aviation and Missile Research Development and Engineering Center.

#238453 Received 22 Apr 2015; revised 10 Jun 2015; accepted 19 Jun 2015; published 4 Aug 2015